



Reduction Reactions on Iron Sulfides in Aqueous Acidic Solutions

Saba Navabzadeh Esmaeely^z and Srdjan Nesic

Institute for Corrosion and Multiphase Flow Technology, Department of Chemical and Biomolecular Engineering, Ohio University, Athens, Ohio 45701, USA

Iron sulfide corrosion product layers commonly form on mild steel surfaces corroding in aqueous H₂S environments. These porous layers present a barrier which may reduce the corrosion rate, however, their semi-conductive nature leads to an acceleration of corrosion via galvanic coupling, by increasing the cathodic surface area. The electrocatalytic properties of different iron sulfides, which are important in this process, were unknown. The current study looks at the cathodic reaction rates on the surfaces of geological pyrite, geological pyrrhotite, and mild steel in HCl, CO₂ and H₂S aqueous solutions at different pH. Results show that in solutions where H⁺ reduction dominates, pyrite has similar electroactivity as X65 steel, while pyrrhotite exhibits approximately one order of magnitude smaller current densities. An extra wave observed in the cathodic sweeps on pyrrhotite was due to conversion of pyrrhotite to troilite. In aqueous CO₂ solutions, similar results were obtained, while in H₂S aqueous environments, both pyrite and pyrrhotite showed similar electroactivity that was slightly lesser than that of X65 steel.

© The Author(s) 2017. Published by ECS. This is an open access article distributed under the terms of the Creative Commons Attribution Non-Commercial No Derivatives 4.0 License (CC BY-NC-ND, <http://creativecommons.org/licenses/by-nc-nd/4.0/>), which permits non-commercial reuse, distribution, and reproduction in any medium, provided the original work is not changed in any way and is properly cited. For permission for commercial reuse, please email: oa@electrochem.org. [DOI: 10.1149/2.1381712jes] All rights reserved.



Manuscript submitted June 26, 2017; revised manuscript received August 21, 2017. Published August 30, 2017. This article is a version of Paper 686 from the National Harbor, Maryland Meeting of the Society, October 1–5, 2017.

Iron sulfides can be found in various forms, the most common being: mackinawite (FeS) that has a tetragonal crystalline structure, cubic ferrous sulfide (FeS), troilite (FeS) with a hexagonal structure, polymorphous pyrrhotite (Fe_{1-x}S), hexagonal smythite (Fe_{3+x}S₄), cubic greigite (Fe₃S₄), cubic pyrite (FeS₂) and orthorhombic marcasite (FeS₂).¹ They contain iron in different oxidation states (Fe²⁺ and Fe³⁺), with a broad range of non-stoichiometric compositions and have distinct physicochemical and electrical properties. Iron sulfides are classified as semiconductors¹ with their electrochemistry being an important area of investigation across different fields of application, including clean energy related research,^{2–6} corrosion of steel in H₂S containing environments,^{7–12} geochemical studies,^{12–15} etc. For example pyrite, and pyrrhotite are two most abundant iron sulfides found in the Earth's crust^{1,16–18} and are at the same time among the most common corrosion products of steel corrosion due to H₂S.

Pyrite is the most thermodynamically stable stoichiometric iron sulfide,¹ having the lowest solubility in water as compared to other iron sulfides.¹⁹ Pyrite is a semiconductor with a resistivity in the range of 10⁻⁵ – 10¹ Ωm^{20–22} and is found as both n-type and p-type.²³ Pyrrhotite (Fe_(1-x)S (x = 0–0.2))^{17,24–27} is an iron deficient iron sulfide, with a crystalline structure changing from monoclinic to hexagonal depending on its iron deficiency. For example, hexagonal stoichiometric pyrrhotite is known as troilite. Both pyrrhotite and troilite are p-type semiconductors with a resistivity^{20–22} in the range of 10⁻⁶ – 10⁻¹ Ωm.¹

The electrochemistry of iron sulfides investigated to date, has been mostly focused on anodic reactions, such as phase transformation and dissolution^{28–32} which are predominantly important in weathering of iron sulfides in nature, oxidation during mining^{33,34} and transportation and metal extraction.^{28,29,35} Other researchers in the same field focused almost exclusively on O₂ reduction on the surface of iron sulfides, which is the most important cathodic process in such systems.^{36–38} Limited work has been reported on cathodic reactions in acidic media. In a study that was mostly focused on iron sulfide dissolution by both anodic and cathodic currents, Peters³⁰ stated that pyrite facilitates H⁺ reduction due to its low overpotential. Some additional information on rates of hydrogen evolution on iron sulfide surfaces was reported in fuel cell related research, where it was found that pyrite is more active than greigite and pyrrhotite.^{5,39}

The formation of iron sulfide corrosion product layers on mild steel corroding in aqueous H₂S environment is common across a broad range of conditions. These porous layers offer some degree of

protection by presenting a diffusion barrier and by covering the steel surface, leading to retardation in anodic dissolution of iron. However, the semi-conductive nature of the iron sulfide of the corrosion product layers could also result in an acceleration of corrosion by significantly increasing the surface area for the cathodic reactions, leading to a galvanic coupling.⁴⁰ The significance of this effect remains unclear since the electrocatalytic properties of different iron sulfides are unknown. Furthermore, the presence of different iron sulfide layers has been associated with onset of localized corrosion.^{8,41–43} The exact mechanism behind this phenomenon is not yet clear. One possible explanation is related to different electroactivity of the various iron sulfides. Therefore, understanding of the rate of cathodic reduction of corrosive species in acidic media on different iron sulfide surfaces, as compared to steel, is of crucial importance. The current study covers an investigation of the cathodic reaction rates on the surfaces of pyrite, pyrrhotite, troilite, and mild steel in HCl, CO₂ and H₂S aqueous solutions at different pH.

Experimental

Experiments were carried out in a glass cell containing 2 liters of deionized water (DI) and 20.2 gram analytical grade sodium chloride (NaCl). The key experimental conditions are summarized in Table I. Prior to each experiment, the solution was deoxygenated with N₂ or CO₂ gas for at least 3 hours. For the H₂S experiments, following the N₂ purge, H₂S was added to the gas stream introduced into the glass cell. The gas flow was maintained continuously throughout the duration of

Table I. Experimental Matrix.

Parameters	Conditions	
Total pressure	0.1 MPa	
Temperature	30°C	
Solution	1 wt% NaCl	
Test condition	250, 1000 rpm	
Material	API 5L X65, pyrite, pyrrhotite, troilite	
Methods	EIS, and Potentiodynamic Sweep	
Purged gas	HCl solution	0.096 MPa N ₂
	aqueous CO ₂ solution	0.096 MPa CO ₂
	aqueous H ₂ S solution	0.01 MPa H ₂ S, 0.086 MPa N ₂
pH value	2.0, 3.0, 4.0 and 5.0 (± 0.1)	

^zE-mail: sn294410@ohio.edu

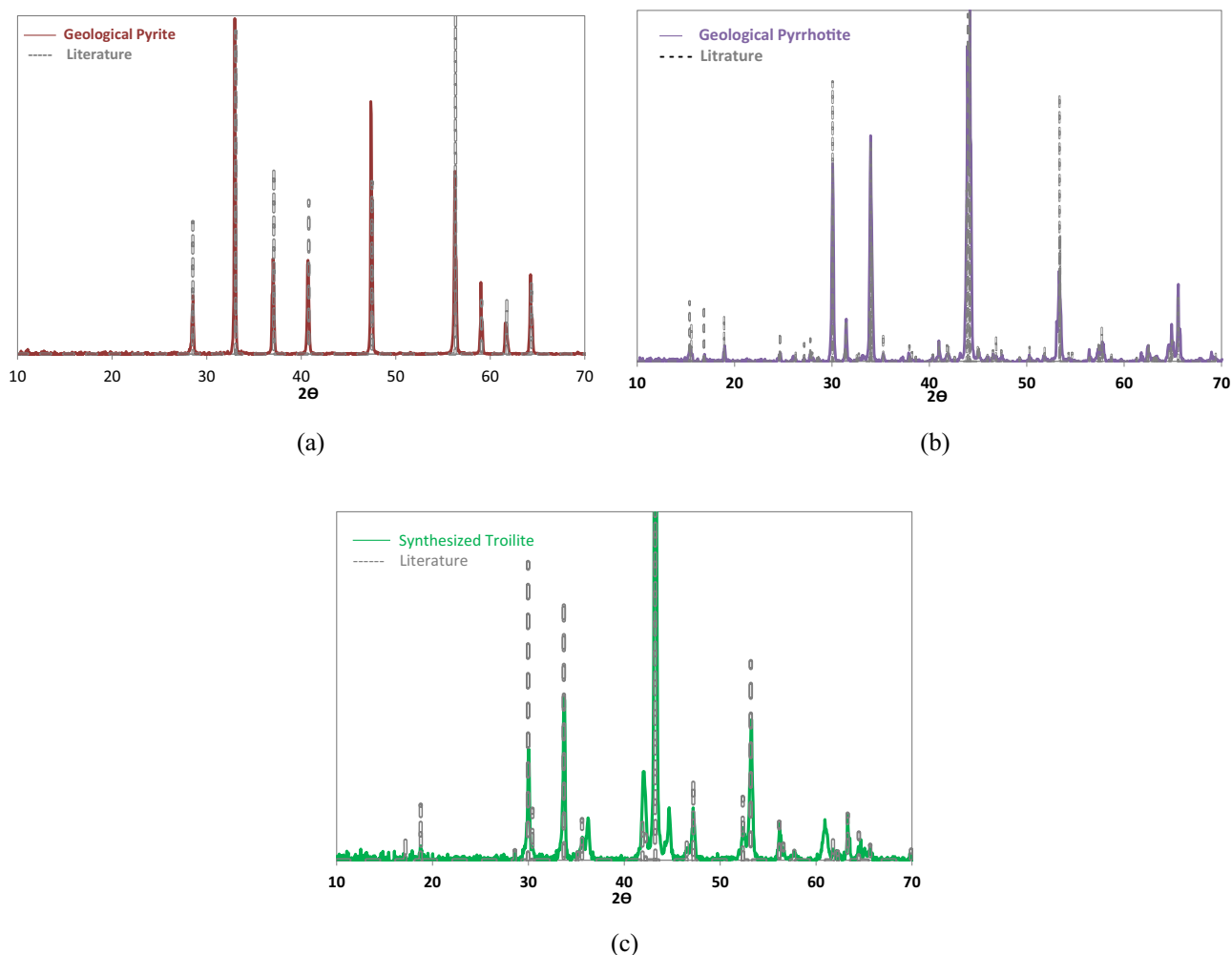


Figure 1. XRD data (a) geological pyrite (b) geological pyrrhotite (c) synthesized troilite.

the experiments. Upon exiting the glass cell, the gas containing H_2S was scrubbed by using a 5 molL^{-1} sodium hydroxide (NaOH) solution and multiple dry carbon scrubbers. The solution pH was monitored by an OMEGA 5992-02 pH probe, deoxygenated hydrochloric acid (HCl) or NaOH solution was used to adjust the pH.

Four different types of working electrode were used in the current study, made from: API 5L X65 steel, geological specimens of pyrite and pyrrhotite, and synthesized troilite. Scientific grade pyrite was purchased from Alfa Aesar, pyrrhotite specimens were provided by Ward's Science and synthesized troilite was purchased from Merck Group. XRD analyses were conducted on the powdered samples of the iron sulfides to assure that there were no substantial impurities present. The results of XRD analyses are shown in Figure 1 confirming that the specimens did not contain any appreciable amount of impurities.

The X65 steel electrode was machined into a disc with a diameter of 5 mm and mounted onto a rotating disc Teflon holder. To make the iron sulfide electrodes, iron sulfide particles 3 to 7 mm in size were selected; they were palladium (Pd) coated on one side and connected to a wire using a silver paste, then embedded in a clear epoxy and mounted onto a rotating disc Teflon holder. The Pd coat was implemented to enhance the wiring connection with the iron sulfide surface, and minimize ohmic drop, which could interfere with the electrochemical measurements. The specimens were then sequentially abraded and polished down to a finish obtained with a $0.25 \mu\text{m}$ diamond suspension, rinsed with DI water and cleaned with alcohol in an ultrasonic bath. Then they were dried using N_2 and photographed. Soon after, they were inserted into the experimental cell so that the

exposure to air was minimized in order to avoid any oxide formation. The photographs were processed using ImageJ open source software, in order to determine the irregularly shaped surface area of the iron sulfide working electrodes. Due to the deviation from a perfect circle, some discrepancy between measured and calculated limiting current densities was to be expected.

Electrochemical measurements were conducted using a Gamry Reference 600 potentiostat on rotating disc electrodes (RDEs) in a conventional three electrode setup, where a platinum mesh was used as a counter electrode and a saturated silver/silver chloride (Ag/AgCl) reference electrode, connected via a KCl salt bridge and a Luggin capillary. Open circuit potential (OCP) measurements were conducted prior to each potentiodynamic sweep, in order to make sure that it was stable, which took typically less than 5 minutes. X65 steel exposed to H_2S environment is subject to formation of iron sulfide in H_2S environments, given the relatively fast kinetics of reactions in such environments. However, due to a short term exposure before each potentiodynamic sweep, the possible interference of the iron sulfide layer on the measurements was minimized as previously demonstrated.^{44,45} Electrochemical impedance spectroscopy (EIS) (DC potential 0 mV vs. OCP, AC potential 10 mV, frequency range 10 KHz to 1 Hz at 10 points/dec), was performed in order to determine the ohmic drop in the solution at high frequencies (ca. 10 KHz), which was used to correct the raw potentiodynamic sweep data. Potentiodynamic sweeps were performed by polarizing the working electrode from the OCP in the cathodic direction at a scan rate of 1 mVs^{-1} . The potentiodynamic sweeps were repeated at least three times for each condition, in

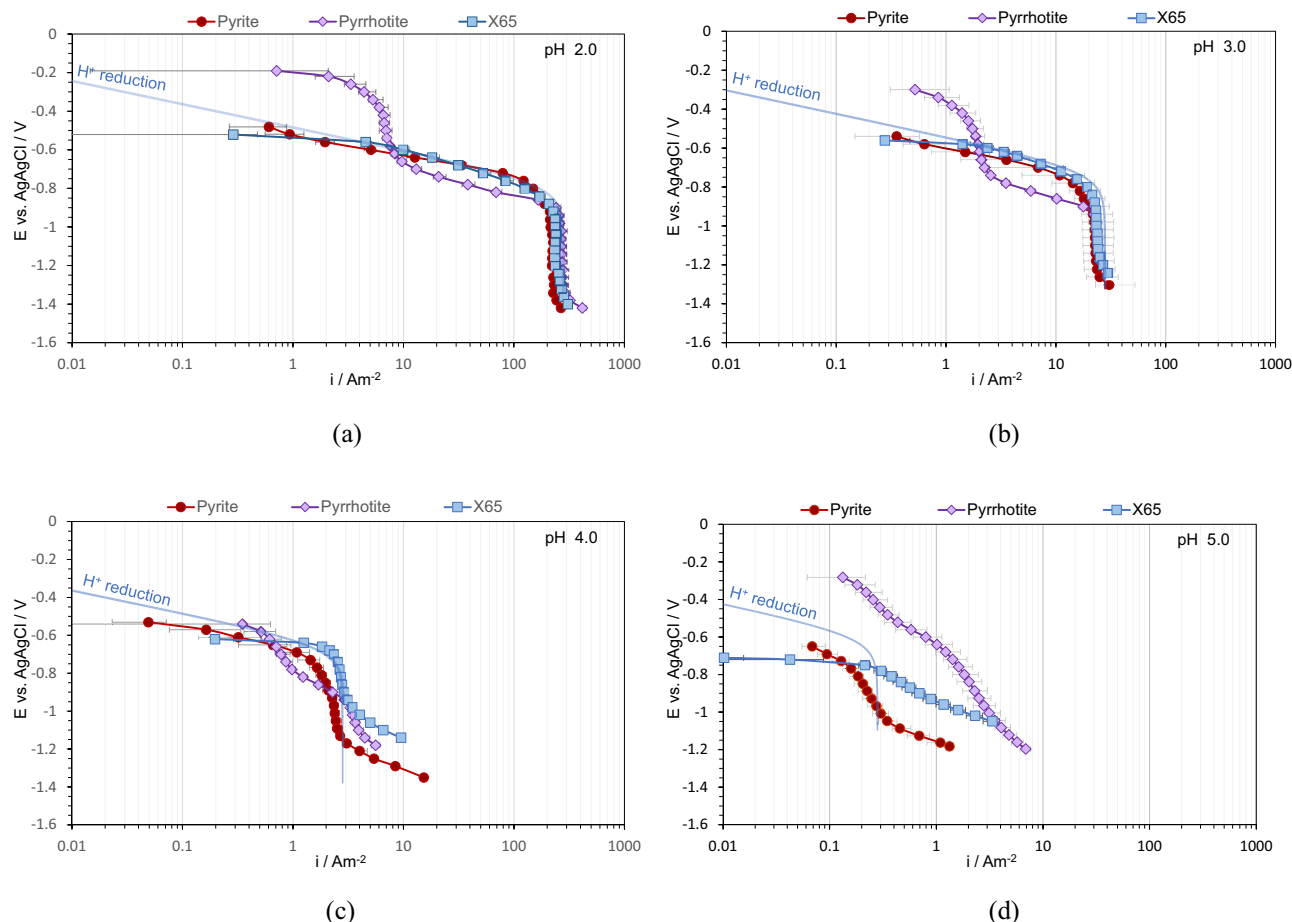


Figure 2. Potentiodynamic sweeps on X65 mild steel, pyrite, and pyrrhotite in N_2 purged solutions, 1 wt% NaCl, 30°C, and 1000 rpm RDE, scan rate 1 mVs^{-1} , (a) pH 2.0, (b) pH 3.0, (c) pH 4.0 (d) pH 5.0.

some cases without removing the electrode from the solution and in other cases by using freshly polished electrodes in a newly prepared solution. The data reported below are the averages obtained in multiple repeats.

Results and Discussion

HCl aqueous solutions.—In the first series of experiments shown in Figure 2, cathodic sweeps were obtained on pyrite, pyrrhotite, and X65 steel in NaCl + HCl aqueous solutions purged by N_2 at pH 2.0, pH 3.0, pH 4.0, and pH 5.0; the data were collected at room temperature. The points shown represent the average value of the current density obtained in different repeats at the same potential, while the error bars denote the maximum and minimum values. The lines represent the calculated current density for H^+ reduction on a mild steel surface obtained by using an electrochemical model previously proposed by Zheng et al.⁴⁶ and Esmaeely et al.⁴⁵

In the current series of experiments, H^+ reduction was considered as the main cathodic reaction:



and water reduction was neglected.

In the HCl solution at pH 2.0 and pH 3.0, the pyrite surface showed similar electroactivity as the X65 steel surface (Figures 2a and 2b). A full overlap of the H^+ reduction curves can be seen in both the charge transfer and the mass transfer controlled regions, agreeing well with the model. However, the charge transfer rate for H^+ reduction on pyrrhotite was approximately an order of magnitude slower, while the limiting current density was the same as on pyrite and X65 steel.

Since the limiting current density is mass transfer controlled, one would expect that it is independent of the nature of the substrate. At pH 4.0 this behavior was not as obvious, while at pH 5.0 no clear limiting current density could be observed and the electroactivity of the different surfaces does not appear to follow the trend seen at lower pH (Figures 2c and 2d). This will be discussed in more details further below.

At pH 2.0, pH 3.0, and pH 4.0 the potentiodynamic sweeps on pyrrhotite showed an extra “wave”, with a limiting current density in the range much smaller than what was observed for H^+ mass transfer. In order to understand the nature of the reduction reaction behind this extra wave, the potentiodynamic sweeps were conducted on pyrrhotite at different pH as shown in Figure 3. It can be observed that the position of this wave changes with pH, with a limiting current density decreasing at higher pH values. This was further investigated by conducting potentiodynamic sweeps at different rotational speeds, as shown in Figure 4. There it can be seen that the limiting current densities for both H^+ reduction and the extra wave approximately halved when the rotational speed decreased by a factor of 4. This is consistent with the RDE mass transfer limiting current density expression defined by Levich.

$$i_L = (0.620)nFD^{\frac{2}{3}}\omega^{\frac{1}{2}}\nu^{-\frac{1}{6}}C \quad [2]$$

where i_L is the mass transfer limiting current density ($A \text{ m}^{-2}$), n is the number moles of electrons transferred in the half reaction, F is the Faraday’s constant ($C \text{ mol}^{-1}$), D is the diffusion coefficient ($\text{m}^2 \text{ s}^{-1}$), ω is the rotational velocity (rad s^{-1}), ν is the kinematic viscosity ($\text{m}^2 \text{ s}^{-1}$), and C is the concentration of the reactant (mol m^{-3}).

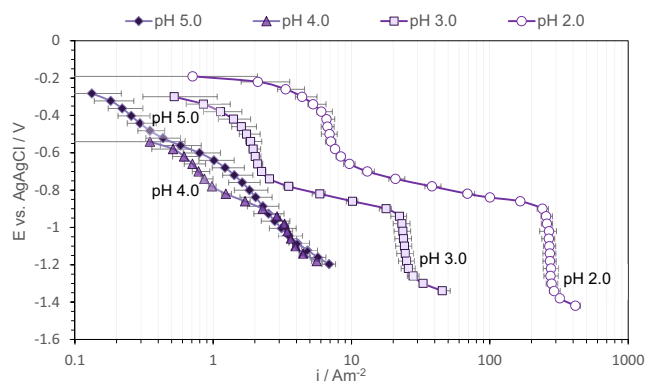
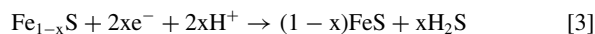


Figure 3. Potentiodynamic sweeps on pyrrhotite in N_2 purged solutions, 1 wt% NaCl, 30°C, scan rate 1 mVs^{-1} , 1000 rpm at different pH.

These experiments provided evidence that the extra wave obtained on the pyrrhotite surface was related, at least in part, to bulk conditions. Considering that in a deoxygenated HCl solution the only reducible species are H^+ and H_2O , the reaction behind the extra wave must have involved H^+ as one of the reactants. Given that the extra wave was seen only on pyrrhotite it was presumed that the reaction involved both pyrrhotite and the H^+ ions. Nicol et al.⁴⁷ and Mikhlin et al.⁴⁸ proposed that the following reactions take place upon pyrrhotite exposure to an acidic solution: pyrrhotite first reduces to troilite, followed by the chemical dissolution of troilite with release of H_2S .



The first reduction Reaction 3 is pH dependent, with an H^+ dependency order of $2x$ (where $x = 0 - 0.2$ is the extent of Fe^{2+} deficiency in the pyrrhotite crystal lattice).²⁵ This reaction proceeds faster at higher H^+ concentrations. Therefore, it is here hypothesized that the extra wave was due to reduction of pyrrhotite to troilite according to Reaction 3. The pH and velocity dependency shown in Figure 3 and Figure 4, as well as the order of the reaction are all consistent with this hypothesis.

To confirm that the extra wave is reduction of pyrrhotite to troilite, potentiodynamic sweeps were repeated on troilite electrodes. Results obtained at two different pH values are compared with the ones from a pyrrhotite electrode in Figure 5. The absence of the extra wave on troilite and the overlap of the sweeps at both pH values provided con-

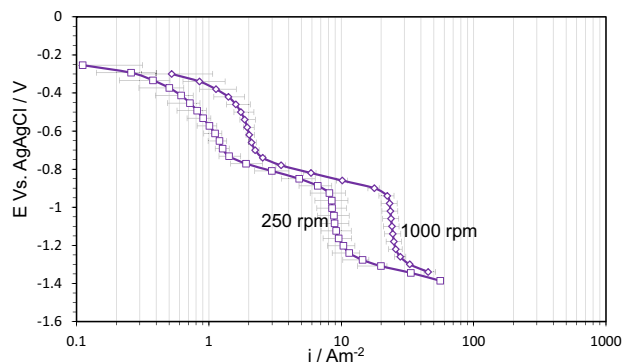


Figure 4. Potentiodynamic sweeps on pyrrhotite in N_2 purged solutions, 1 wt% NaCl, 30°C, scan rate 1 mVs^{-1} , pH 3.0, at different rotational velocity.

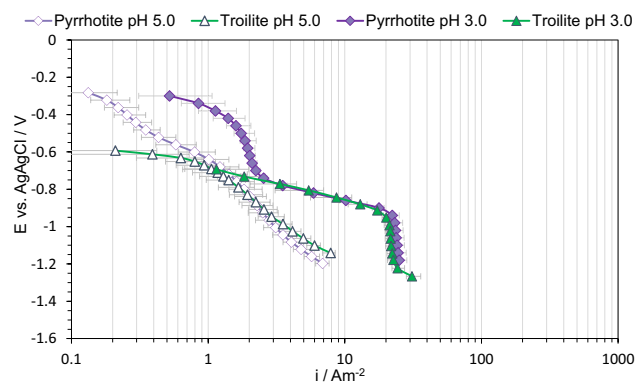


Figure 5. Potentiodynamic sweeps on pyrrhotite and troilite in N_2 purged solutions, 1 wt% NaCl, 30°C, scan rate 1 mVs^{-1} , different pH at 1000 rpm.

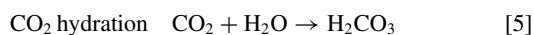
vincing evidence for the abovementioned assumption. Therefore, we can conclude that upon cathodic polarization the surface of pyrrhotite converts to troilite, and the H^+ reduction on pyrrhotite and troilite surfaces proceeds at practically the same rates.

It should be noted that XRD analysis was not conducted to investigate this transformation process, due to the very thin surface layer of troilite that would have formed. As a result, conventional XRD would not be able to detect such a thin layer of troilite. More sensitive techniques such as XPS would be required for such analyses. Furthermore, preservation of the specimen surface following the removal from the experimental cell and during the ex-situ analyses poses additional challenges that would have made the results questionable.

In all experiments conducted on iron sulfide electrodes, another minor “wave” was obtained in the potentiodynamic sweeps at very low current densities in the OCP range for the iron sulfides, not shown in the graphs; this was presumed to be related to the impurities present at the surface of the electrodes, thus it was ignored. Peters and Majima also observed similar behavior during polarization of iron sulfides and attributed it to minor impurities in the parent material.^{29,30}

The electroactivity of pyrite at higher pH values (pH 4.0 and pH 5.0) slightly decreased when compared to X65 steel (Figures 2c and 2d) and the reason behind this behavior is unclear. Pyrrhotite at pH 4.0 showed similar behavior to that seen at lower pH values, however, at pH 5.0, the potentiodynamic sweeps on pyrrhotite were very different, as it appeared that there is an acceleration of the H^+ reduction. It is believed that this is an experimental artifact and is the result of H_2S production due to pyrrhotite conversion to troilite and troilite dissolution according to Reaction 3 and Reaction 4. The produced H_2S , in the vicinity of the electrode surface alters the surface pH through a buffering effect. Moreover, produced H_2S at the surface can be reduced, which leads to even larger overall cathodic current densities. At pH 2.0, pH 3.0, and even pH 4.0, due to a considerably higher H^+ concentration, the generation of a small amount of H_2S did not produced a significant interference. In summary, the potentiodynamic sweeps obtained at pH 4.0 and particularly at pH 5.0 should be interpreted with this in mind.

Aqueous CO_2 solution.—In an aqueous CO_2 solutions, CO_2 hydration results in carbonic acid (H_2CO_3) formation (Reaction 5). H_2CO_3 is a weak acid that contributes to the corrosion process through the buffering effect (Reaction 7) where additional H^+ ions are produced and possibly via direct reduction at the electrode surface (Reaction 6). The direct reduction of H_2CO_3 mechanism was broadly accepted over the past forty years.⁴⁹ However, it was challenged in recent years.⁵⁰⁻⁵² The exact mechanism of H_2CO_3 reduction remains open to discussion; in the current study, it was assumed that in addition to H^+ reduction there was a direct reduction of H_2CO_3 . The H_2O reduction was not considered here.



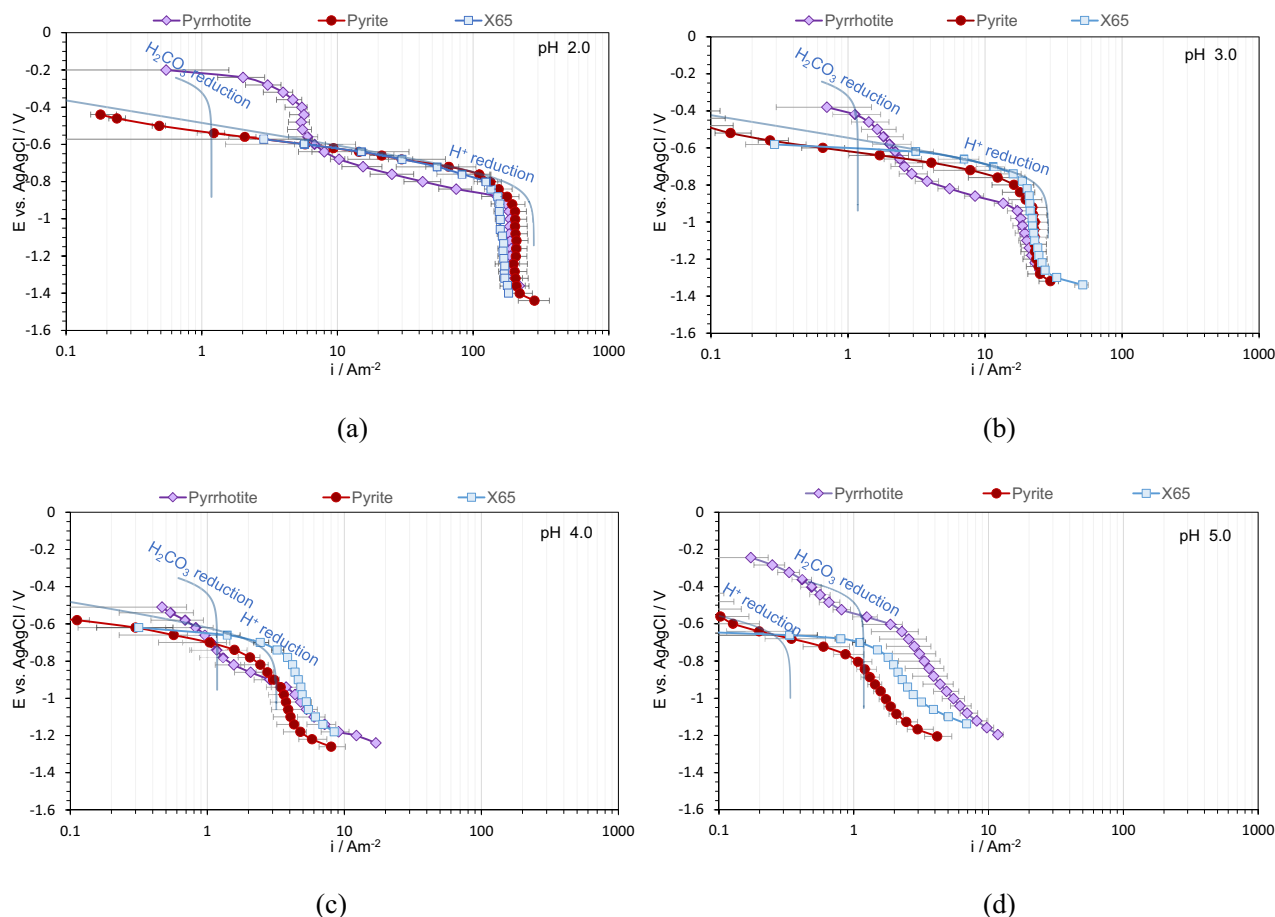
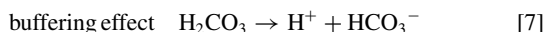
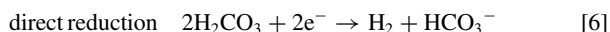


Figure 6. Potentiodynamic sweeps on X65 mild steel, pyrite and pyrrhotite in CO_2 purged solutions, 1 wt% NaCl, 30°C , 1000 rpm, scan rate 1 mVs^{-1} , (a) pH 2.0, (b) pH 3.0, (c) pH 4.0 (d) pH 5.0.



Similar behavior to what was observed in HCl experiments was observed in aqueous CO_2 solutions (Figure 6). At lower pH values pyrite showed similar electroactivity to what was obtained on X65 steel when exposed to the same condition. The measured current densities on pyrrhotite surfaces, were approximately one order of magnitude smaller. The extra wave attributed to reduction of pyrrhotite to troilite was also present across all the experimental conditions in aqueous CO_2 solutions. At pH 2.0 and pH 3.0, the cathodic reaction was dominated by H^+ reduction, just like what was seen in HCl solutions at the same pH, as indicated by the lines generated using the model. At pH 4.0 and pH 5.0, the potentiodynamic sweeps are more complicated to interpret in the same way as they were in HCl solutions without CO_2 . At pH 4.0, the rate of reactions on pyrite appears to be somewhat slower than on X65 steel, for reasons that are not well understood. The same is true at pH 5.0, however, it also seems that the reactions on pyrrhotite are greatly accelerated at this pH. Just like in HCl solutions, this is an artifact of the experimental conditions, where small amounts of H_2S produced by conversion of pyrrhotite to troilite and troilite dissolution (Reaction 3 and Reaction 4 respectively) were immediately reduced leading to higher current densities.

Aqueous H_2S solution.—In aqueous H_2S solutions, in addition to H^+ reduction, the dissolved H_2S is also directly reduced on the surface

of the electrode (Reaction 8), which manifests itself in the form of an extra wave on the potentiodynamic sweeps. This was discussed in detail in recent publications by Zheng et al.,^{44,46} Kittel et al.⁵³ and Esmaeely et al.⁴⁵



Potentiodynamic sweeps conducted at pH 2.0 in an aqueous H_2S solution are shown in Figure 7a, where the dominant cathodic reaction was H^+ reduction. The relatively large error in the measured limiting current could be attributed to the irregular surface geometry of the electrodes as was noted above. There, similar behavior was seen to what was observed in HCl solution shown in Figure 5a; reduction rates of H^+ on pyrite and mild steel overlapped, while on pyrrhotite approximately one order of magnitude smaller current density was observed. The extra wave related to reduction of pyrrhotite to troilite was also present. However, at higher pH values, the H_2S reduction is dominant (Figures 7b–7d). There, it is observed that the H_2S reduction rate is slightly lower (2 to 3 times) on both pyrite and pyrrhotite as compared to the rate on the X65 steel surface. Thus, the H^+ reduction wave, which was overpowered by the H_2S reduction on X65 steel, was observable on both pyrite and pyrrhotite (Figures 5b–5d). The H_2S reduction rates on pyrrhotite and pyrite were approximately the same. The pyrrhotite to troilite reduction wave was consistently present across all the experimental conditions. However, in aqueous H_2S solutions the artifact related to H_2S production as a result of the reduction of pyrrhotite to troilite and troilite dissolution, which were observed in the HCl and aqueous CO_2 solution, was not observed here; the small amounts of produced H_2S were negligible in H_2S saturated solutions.

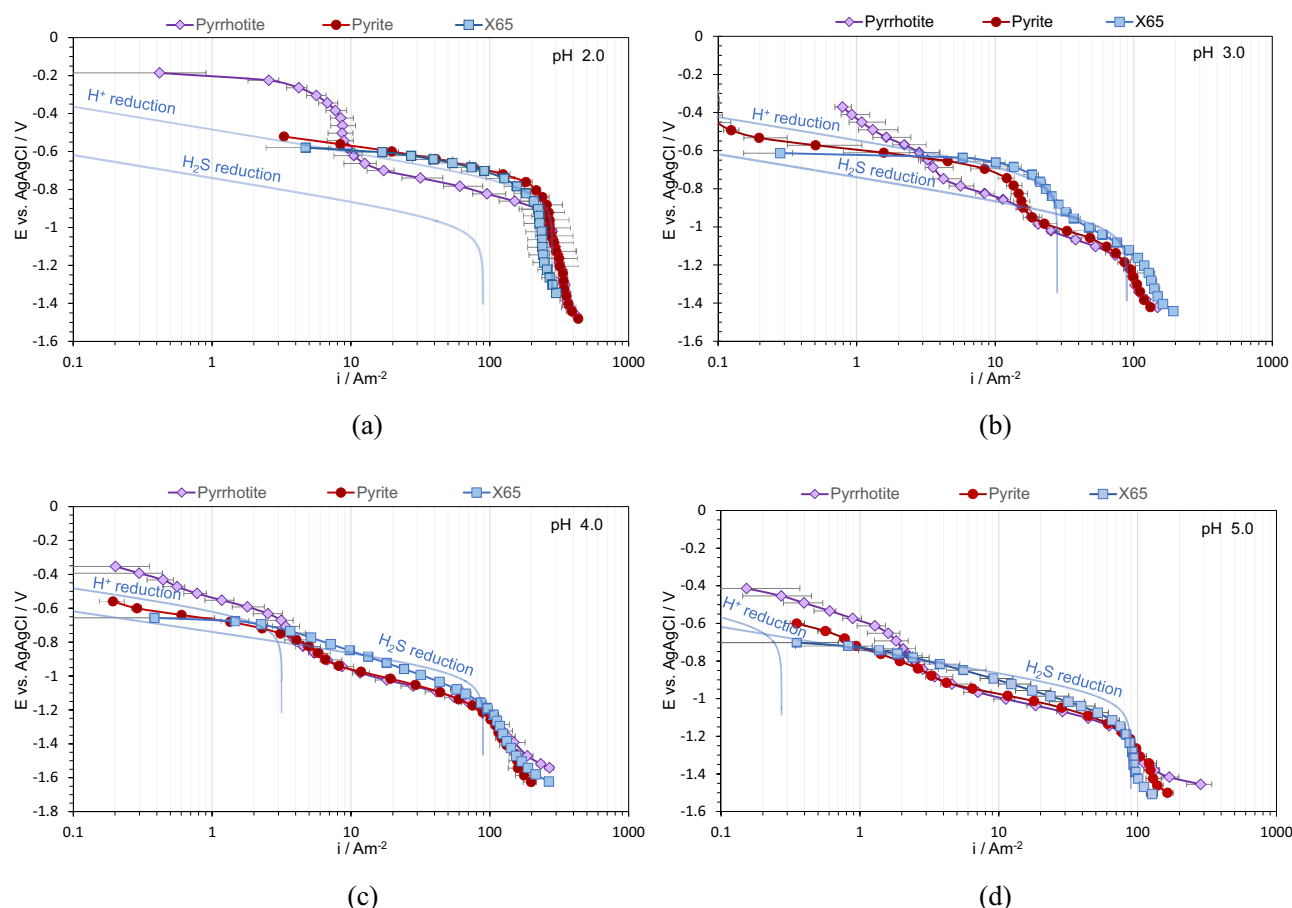


Figure 7. Potentiodynamic sweeps on X65 mild steel, pyrite, and pyrrhotite in aqueous solutions with 0.01 MPa H_2S , 1 wt% NaCl, 30°C, 1000 rpm, scan rate 1 mVs^{-1} , (a) pH 2.0, (b) pH 3.0, (c) pH 4.0, (d) pH 5.0.

Conclusions

Cathodic potentiodynamic sweeps were conducted on the surfaces of different iron sulfides including pyrite, pyrrhotite and troilite in deoxygenated acidic aqueous solutions. A comparison of the data obtained on iron sulfides with what was observed on X65 steel showed that in conditions dominated by H^+ reduction, pyrite had similar electroactivity as the steel. There was some minor deviation at pH 4.0 and pH 5.0, for reasons that remain unclear. In the same conditions, the cathodic current densities obtained on pyrrhotite were almost the same and approximately one order of magnitude smaller than what was observed on pyrite and X65 steel. Cathodic sweeps data on pyrrhotite showed an extra wave at the lower current densities obtained at more positive range of potentials, which was identified to be due to pyrrhotite reduction to troilite. In aqueous CO_2 solutions, similar results were obtained as in HCl solutions. In H_2S containing aqueous environments, both pyrite and pyrrhotite showed similar electroactivity with corrosion current densities that were slightly smaller than what was measured on X65 steel.

Acknowledgment

The authors acknowledge the financial support from a joint industry project including BP, Champion Technologies, Chevron, ConocoPhillips, DNV GL, ENI S.p.A., ExxonMobil, Hess, MultiChem, NALCO Energy Services, Occidental Petroleum Co., Petrobras, PETRONAS, PTT, Saudi Aramco, Inpex Corporation, SINOPEC, TOTAL, TransCanada, WIGIM, Shell. The authors would like to express their appreciation to Dr. Bert Pots, Dr. Bruce Brown and Aria Kahyarian for their contributions to this work.

References

1. D. J. Vaughan and J. R. Craig, *Mineral chemistry of metal sulfides*, p. 17, first ed., Vail-Ballou, New York (1978).
2. Y. Bi, Y. Yuan, C. L. Exstrom, S. A. Darveau, and J. Huang, "Air stable, photosensitive, phase pure iron pyrite nanocrystal thin," *Nano Lett.*, 4953 (2011).
3. M. Cabán-Acevedo, M. S. Faber, Y. Tan, R. J. Hamers, and S. Jin, "Synthesis and properties of semiconducting iron pyrite (FeS_2) nanowires," *Nano Lett.*, 12, 1977 (2012).
4. A. Ennaoui, S. Fiechter, Ch. Pettenkofer, N. Alonso-Vante, K. Buker, M. Bronold, Ch. Hopfner, and H. Tributsch, "Iron disulfide for solar-energy conversion," *Sol. Energy Mater. Sol. Cells*, 29, 289 (1993).
5. C. Di Giovanni, W. Wang, S. Nowak, J. Grenèche, H. Lecoq, L. Mouton, M. Giraud, and C. Tard, "Bioinspired iron sulfide nanoparticles for cheap and long-lived electrocatalytic molecular hydrogen evolution in neutral water," *ACS Catal.*, 4, 681 (2014).
6. A. L. Quachukwu, "Hydrogen evolution on iron pyrite (FeS_2) in sodium chloride solution," *Electrochim. Acta*, 27, 529 (1982).
7. W. Sun, S. Nestic, and S. Papavinasam, "Kinetics of corrosion layer formation. part 2-iron sulfide and mixed iron sulfide/carbonate layers in carbon dioxide / hydrogen sulfide corrosion," *Corrosion*, 64, 586 (2008).
8. J. Ning, Y. Zheng, B. Brown, D. Young, and S. Nestic, "The role of iron sulfide polymorphism in localized H_2S corrosion of mild steel," *Corrosion*, 73, 155 (2017).
9. S. Gao, P. Jin, B. Bruce, D. Young, and S. Nestic, "Corrosion behavior of mild steel in sour environments at elevated temperatures," *Corrosion*, (2017).
10. H. Ma, X. Cheng, G. Li, S. Chen, Z. Quan, S. Zhao, and L. Niu, "The influence of hydrogen sulfide on corrosion of iron under different conditions," *Corros. Sci.*, 42, 1669 (2000).
11. H. Vedage, T. A. Ramanarayanan, J. D. Mumford, and S. N. Smith, "Electrochemical growth of iron sulfide films in H_2S -saturated chloride media," *Corrosion*, 49, 114 (1993).
12. D. Rickard and G. W. Luther, "Chemistry of iron sulfides," *Chem. Rev.*, 107, 514 (2007).
13. J. Morse, F. Millero, J. Cornwell, and D. Rickard, "The chemistry of the hydrogen sulfide and iron sulfide systems in natural waters," *Earth-Science Rev.*, 24, 1 (1987).
14. R. Murphy and D. R. Strongin, "Surface reactivity of pyrite and related sulfides," *Surf. Sci. Rep.*, 64, 1 (2009).

15. J. M. Guevremont, J. Bebie, A. R. Elsetinow, D. R. Strongin, and M. A. A. Schoonen, "Reactivity of the (100) plane of pyrite in oxidizing gaseous and aqueous environments: effects of surface imperfections," *Environ. Sci. Technol.*, **32**, 3743 (1998).
16. M. F. Cai, Z. Dang, Y. W. Chen, and N. Belzile, "The passivation of pyrrhotite by surface coating," *Chemosphere*, **61**, 659 (2005).
17. N. Belzile, Y. W. Chen, M. F. Cai, and Y. Li, "A review on pyrrhotite oxidation," *J. Geochemical Explor.*, **84**, 65 (2004).
18. P. H. Tewari, G. Wallace, and A. B. Campbell, "The solubility of iron sulfides and their role in mass transport," *Whiteshell Nuclear Research Establishment*, **9**, 22 (1978).
19. W. Davison, "The solubility of iron sulfides in synthetic and natural-waters at ambient-temperature," *Aquat. Sci.*, **53**, 309 (1991).
20. W. H. Thomason, Formation rates of protective iron sulfide films on mild steel in H₂S-saturated brine as a function of temperature, no. 41, NACE International, Houston, TX (1978).
21. F. H. Meyer, O. L. Riggs, R. L. McGlasson, and J. D. Sudbury, "Corrosion products of mild steel in hydrogen sulfide environments," *Corrosion*, **14**, 69 (1958).
22. W. Zhao, Y. Zou, K. Matsuda, and Z. Zou, "Characterization of the effect of hydrogen sulfide on the corrosion of X80 pipeline steel in saline solution," *Corrosion Science*, **102**, 455 (2016).
23. E. Ahlberg and A. E. Broo, "Electrochemical reaction mechanisms at pyrite in acidic perchlorate solutions," *Electrochem. Soc.*, **144**, 1281 (1997).
24. J. S. Smith and J. D. A. Miller, "Nature of sulphides and their corrosive effect on ferrous metals: a review," *British Corrosion J.*, **10**, 136 (1975).
25. A. V. Kuklinskii, Y. L. Mikhlin, G. L. Pashkov, V. F. Kargin, and I. P. Asanov, "Conditions for the formation of a nonequilibrium nonstoichiometric layer on pyrrhotite in acid solutions," *Russ. J. Electrochemistry*, **37**, 1458 (2001).
26. Y. L. Mikhlin, A. V. Kuklinskii, G. L. Pashkov, and I. P. Aanov, "Pyrrhotite electrooxidation in acid solutions," *Russ. J. Electrochemistry*, **37**, 1466 (2001).
27. Y. L. Mikhlin, V. Varnek, I. Asanov, Y. Tomashevich, A. Okotrub, A. Livshits, G. Selyutin, and G. Pashkov, "Reactivity of pyrrhotite (Fe₉S₁₀) surfaces: spectroscopic studies," *Phys. Chem. Chem. Phys.*, **2**, 4393 (2000).
28. R. E. Meyer, "Electrochemistry of FeS₂," *Electroanal. Chem.*, **101**, 59 (1979).
29. E. Peters and H. Majima, "Electrochemical reactions of pyrite in acid perchlorate solutions," *Canadian Metallurgical Quarterly*, **7**, 111 (1968).
30. E. Peters, in *Trends in Electrochemistry*, J. O. M. Bockris, D. A. J. Rand, and B. J. Welch (Eds.), p. 267 (1977).
31. T. Biegler and D. A. Swift, "Anodic behaviour of pyrite in acid solutions," *Electrochim. Acta*, **24**, 415 (1979).
32. I. C. Hamilton and R. Woods, "An investigation of surface oxidation of pyrite and pyrrhotite by linear potential sweep voltammetry," *Journal of Electroanalytical Chemistry and Interfacial Electrochemistry*, **118**, 327 (1981).
33. D. K. Nordstrom, in *Acid Sulfate Weathering*, D. M. Kral, p. 37, Soil Science Society of America, Wisconsin (1982).
34. P. C. Singer and W. Stumm, "Acidic mine drainage: the rate-determining step," *Science*, **167**, 1121 (1970).
35. N. J. Welham and G. H. Kelsall, "Recovery of gold from pyrite FeS₂ by aqueous chlorination II. reduction of aqueous chlorine on pyrite (FeS₂)," *Electrochemical Society*, **14**, 164 (2000).
36. T. Biegler, D. A. J. Rand, and R. Woods, "Oxygen reduction on sulfide minerals Part I. kinetics and mechanism at rotated pyrite electrodes," *J. Electroanal. Chem.*, **60**, 151 (1975).
37. T. Biegler, "Oxygen reduction on sulfide minerals Part II. relation between activity and semiconducting properties of pyrite electrodes," *Electroanal. Chem.*, **70**, 265 (1976).
38. D. A. J. Rand, "Oxygen reduction on sulfide minerals Part III. comparison of activities of various copper, iron, lead and nickel mineral electrodes," *Electroanal. Chem.*, **83**, 19 (1977).
39. C. Di Giovanni, A. R. eyes-Carmona, A. Coursier, S. Nowak, J.-M. Greneche, H. Lecoq, L. Mputon, J. Roziere, D. Jones, J. Peron, M. Giraud, and C. Tard, "Low-cost nanostructured iron sulfide electrocatalysts for PEM water electrolysis," *ACS Catal.*, **6**, 2626 (2016).
40. R. L. Pozzo and I. Iwasaki, "Electrochemical Study of Pyrrhotite-Grinding Media Interaction Under Abrasive Conditions," *Corrosion*, **43**, 159 (1987).
41. O. Yezpe, N. Obeyesekere, and J. Wylde, *Study of sour corrosion mechanism under controlled pH*, no. 7795, NACE International, Houston, TX (2016).
42. J. Kvarekvål and G. Svenningsen, *Effect of iron sulfide deposits on sour corrosion of carbon steel*, no. 7313, NACE International, Houston, TX (2016).
43. M. Tjeltha and J. Kvarekvål, *Electrochemistry of iron sulfide and its galvanic coupling to carbon steel in sour aqueous solution*, no. 7478 NACE International, Houston, TX (2016).
44. Y. Zheng, B. Brown, and S. Nešić, "Electrochemical study and modeling of H₂S corrosion of mild steel," *Corrosion Science*, **70**, 351 (2014).
45. S. N. Esmaeely, B. Brown, and S. Nestic, "Verification of an electrochemical model for aqueous corrosion of mild steel for H₂S partial pressures up to 0.1 MPa," *Corrosion*, **73**, 144 (2017).
46. Y. Zheng, J. Ning, B. Brown, and S. Nešić, "Electrochemical model of mild steel corrosion in a mixed H₂S/CO₂ aqueous environment in the absence of protective corrosion product layers," *Corrosion*, **71**, 316 (2015).
47. M. J. Nicol and S. D. Scott, "The kinetics and mechanism of the non-oxidative dissolution of some iron sulphides in aqueous acidic solutions," *J. South African Inst. Min. Metall.*, 298 (1979).
48. Y. Mikhlin, "Reactivity of pyrrhotite surfaces: an electrochemical study," *Phys. Chem. Chem. Phys.*, **2**, 5672 (2000).
49. C. De Waard and D. E. Williams, "Carbonic acid corrosion of steel," *Corrosion*, **31**, 177 (1975).
50. A. Kahyarlan, M. Singer, and S. Nestic, "Modeling of uniform CO₂ corrosion of mild steel in gas transportation systems: a review," *J. Nat. Gas Sci. Eng.*, **29**, 530 (2016).
51. E. Remita, B. Tribollet, E. Sutter, V. Vivier, F. Ropital, and J. Kittel, "Hydrogen evolution in aqueous solutions containing dissolved CO₂: quantitative contribution of the buffering effect," *Corros. Sci.*, **50**, 1433 (2008).
52. T. Tran, *Corrosion Mechanisms of Mild Steel in Weak Acids*, Ph.D. Dissertation, Ohio University (2014).
53. J. Kittel, F. Ropital, F. Grosjean, E. M. M. Sutter, and B. Tribollet, "Corrosion mechanism in aqueous solutions containin dissolved H₂S. Part I: Characterisation of H₂S reduction on a 316L rotating disc electrode," *Corroaion Science*, **66**, 324 (2013).